

Evaluating the Applicability of the Fokker-Planck Equation in Polymer Translocation: A Brownian Dynamics Study

James M. Polson^{1, a)} and Taylor R. Dunn¹

Department of Physics, University of Prince Edward Island, 550 University Ave., Charlottetown, Prince Edward Island, C1A 4P3, Canada

(Dated: 22 August 2021)

Brownian dynamics (BD) simulations are used to study the translocation dynamics of a coarse-grained polymer through a cylindrical nanopore. We consider the case of short polymers, with a polymer length, N , in the range $N = 21 - 61$. The rate of translocation is controlled by a tunable friction coefficient, γ_{0p} , for monomers inside the nanopore. In the case of unforced translocation, the mean translocation time scales with polymer length as $\langle\tau_1\rangle \sim (N - N_p)^\alpha$, where N_p is the average number of monomers in the nanopore. The exponent approaches the value $\alpha = 2$ when the pore friction is sufficiently high, in accord with the prediction for the case of the quasi-static regime where pore friction dominates. In the case of forced translocation, the polymer chain is stretched and compressed on the *cis* and *trans* sides, respectively, for low γ_{0p} . However, the chain approaches conformational quasi-equilibrium for sufficiently large γ_{0p} . In this limit the observed scaling of $\langle\tau_1\rangle$ with driving force and chain length supports the FP prediction that $\langle\tau\rangle \propto N/f_d$ for sufficiently strong driving force. Monte Carlo simulations are used to calculate translocation free energy functions for the system. The free energies are used with the Fokker-Planck equation to calculate translocation time distributions. At sufficiently high γ_{0p} , the predicted distributions are in excellent agreement with those calculated from the BD simulations. Thus, the FP equation provides a valid description of translocation dynamics for sufficiently high pore friction for the range of polymer lengths considered here. Increasing N will require a corresponding increase in pore friction to maintain the validity of the FP approach. Outside the regime of low N and high pore friction, the polymer is out of equilibrium, and the FP approach is not valid.

I. INTRODUCTION

The translocation of polymers through nanometre-sized pores and channels is an important and complex process that has been the subject of a large body of research in recent years.¹⁻³ In part, this interest is due to its relevance to fundamental biological processes, including DNA and RNA transport across nuclear pores, protein transport through membrane channels, genome packing in bacteriophages, and so on.^{4,5} In addition, the development of experimental techniques to detect and characterize translocation at the single-molecule level has been a major force driving activity in this field. Since the pioneering study of Kasianowicz *et al.*⁶ there has been substantial effort devoted to the refinement of these methods using biological⁷⁻¹³ and solid-state¹⁴⁻²⁰ nanopores. Much of this work is inspired by its potential technological applications, notably the development of a nanopore-based device for rapid DNA sequencing.²¹⁻²⁴

Numerous theoretical studies have investigated different aspects of polymer translocation using a variety of analytical and computer simulation methods. One of the first theoretical approaches to translocation was developed by Sung and Park,²⁵ and Muthukumar.²⁶ Here, translocation is treated as a process in which the polymer maintains conformational quasi-equilibrium throughout, and the dynamics are reduced to monitoring the time-dependence of the translocation coordinate, s , the posi-

tion of the monomer inside the pore. The method involves solving the Fokker-Planck (FP) equation using an analytical approximation for the equilibrium free energy function $F(s)$. The method has been reviewed in detail in Ref. 1. Numerous studies have employed the FP approach to study translocation.^{12,25-36} One notable prediction is form of the scaling of the mean first passage time, $\langle\tau\rangle$, with the polymer length, N . Assuming that pore friction dominates, it follows that $\langle\tau\rangle \sim N^2$ for unforced translocation,^{26,34} and $\langle\tau\rangle \sim N/f_d$ in the presence of a strong driving force, f_d . The latter result is consistent with experimental results for ss-DNA translocation through α -hemolysin pores,^{1,6} but is inconsistent with some results for DNA translocation through solid-state nanopores.^{18,37}

The quasi-equilibrium condition, if it holds at all, must eventually break down for sufficiently long polymers.^{38,39} Non-equilibrium conformational behaviour has been directly observed in computer simulations.⁴⁰⁻⁴⁶ In addition, most simulation studies have yielded translocation time scaling exponent values inconsistent with those predicted by the FP method for the quasi-static regime.^{38,39,41,42,47-68} Conformational quasi-equilibrium is only possible when the polymer relaxation time is sufficiently short compared to the translocation time, and this condition is apparently not satisfied in most simulation studies. A notable exception was reported recently in the Langevin dynamics study of non-driven translocation by de Haan and Slater.⁶⁶ Here, the conformational relaxation time was reduced by decreasing the solvent viscosity. At sufficiently low viscosity and fast chain relaxation, a scaling exponent of $\alpha = 2$ was measured

^{a)}Electronic mail: jpolson@upei.ca; Corresponding author

for polymer chains with lengths in the range $N = 25$ – 99 . This was the first confirmation using simulation methods that the FP approach is valid in the limit of sufficiently fast subchain relaxation. The other means of maintaining quasi-equilibrium is by increasing the pore friction and thus slowing the translocation rate. This was demonstrated in a recent study by one of us, in which Monte Carlo (MC) dynamics simulations were used to study the translocation of a hard-sphere chain through a cylindrical nanopore.⁶⁹ In that study, the translocation rate was decreased by decreasing the nanopore width, which increases the effective friction of monomers in the nanopore. The translocation time distributions were compared with those calculated by solving the FP equation using explicitly calculated free energy functions.⁷⁰ The theoretical distributions were fit to the simulation distributions by adjusting the effective diffusion coefficient D appearing in the FP equation. In the limit of sufficiently high pore friction, the quality of the theoretical predictions was generally excellent for physically meaningful values of D .

Generally, the quasi-equilibrium regime is determined by the pore friction and (for driven translocation) the driving force, which affect the translocation rate, as well as polymer length and solvent viscosity, which affect the relaxation rate. Outside this regime, various other theoretical models have been developed to describe the dynamics in the out-of-equilibrium case for non-driven^{52,55,66} and driven^{45,53,59,67,71–76} translocation. Especially noteworthy is the tension propagation (TP) theory for driven translocation pioneered by Sakaue^{71–73,77} and further refined by others.^{45,74} This model was recently extended by Ikonen *et al.*^{67,75,76,78} Unlike the original theory, their Brownian dynamics tension propagation (BDTP) approach is valid for chains of finite length, and also includes a contribution to the total force due to pore friction. Using this method, it was demonstrated that the scaling exponent α exhibits a pronounced dependence on chain length and approached the asymptotic limit of $\alpha = 1 + \nu \approx 1.6$ only at very large N , thus showing that the wide range of α measured in various simulation studies is a finite-size effect.^{67,75} In addition, α was found to decrease with decreasing N and increasing pore friction, apparently tending toward the value of $\alpha = 1$, which is the FP prediction in the case of sufficiently strong driving force.⁷⁵ Thus, the FP predictions may be a limiting case of the more general BDTP theory.

In the present study, we use Brownian dynamics simulation to study translocation of a finitely extensible nonlinear elastic (FENE) model polymer⁷⁹ through a cylindrical nanopore. The translocation rate is controlled by explicit adjustment of the friction of monomers inside the nanopore. This work is largely a continuation of the work in Ref. 69. In addition, it is closely related to the theoretical study of Ref. 75, which also studied the effects of pore friction. We examine both unforced and forced translocation and analyze the translocation time distributions using the FP method together with explicitly calculated

free energy functions. As expected, quasi-static conditions are observed for sufficiently high pore friction and slow translocation, in which limit, however, the simulations became computationally expensive. Consequently, we restrict this study to relatively short polymer chains. In this limit, we find that the translocation dynamics are consistent with FP predictions for sufficiently high nanopore friction.

The remainder of this article is organized as follows. In Sec. II we describe the model used in the simulations. In Sec. III, we review the essential equations of the FP formalism. We also establish the connection between the diffusion coefficient appearing in the FP equation and the relevant parameters of the molecular model. In Sec. IV we describe the MC simulations used to calculate the translocation free energy functions, the details of the BD simulations, and the calculations using the FP equation. In Sec. V the results of the simulations and theoretical calculations are presented. The significance of those results is discussed in Sec. VI.

II. MODEL

The polymer is modeled as a flexible chain of N spherical particles. All particles interact with the repulsive Lennard-Jones potential:

$$u(r) = \begin{cases} u_{\text{LJ}}(r) - u_{\text{LJ}}(r_{\min}), & r < r_{\min} \\ 0, & r \geq r_{\min} \end{cases} \quad (1)$$

where

$$u_{\text{LJ}}(r) = 4\epsilon \left[(\sigma/r)^{12} - (\sigma/r)^6 \right], \quad (2)$$

and where $r_{\min} = 2^{1/6}\sigma$. Bonded monomers also interact with the FENE potential,

$$u(r) = -\frac{1}{2}kr_0^2 \ln(1 - (r/r_0)^2), \quad (3)$$

where r is the interparticle distance, and where $k\sigma^2/\epsilon = 30$ and $r_0 = 1.5\sigma$.

The nanopore is a cylindrical hole of radius R in a barrier of length L . We choose the center of the cylinder to be along the z axis, with $z = 0$ at one end of the pore and $z = L$ at the other. Monomers interact with an interaction site at the nearest point on the barrier or nanopore wall with the potential of Eq. (1). Note that the pore radius is defined such that $R + 0.5\sigma$ is the distance between the nearest interaction site on the pore wall to the centre of the pore. Monomers inside the pore are subject to a constant driving force of f_d for $z \in [0, L]$. Thus, the associated potential energy is:

$$u_d = \begin{cases} 0, & z < 0 \\ f_d z, & 0 \leq z \leq L \\ f_d L, & z \geq L \end{cases} \quad (4)$$

For the Brownian dynamics (BD) algorithm employed in this study and described below in Section IV B, each

particle has an associated friction coefficient, γ . The value of γ depends on the position of the monomer in the pore. Outside the pore, the coefficient has a value γ_0 , while inside the pore, its value is γ_{0p} . The value of γ_{0p} controls the rate of translocation. In this study, we consider the range where $\gamma_{0p} \geq \gamma_0$, i.e. the friction in the pore exceeds that for a monomer outside the pore. To avoid problems with the BD algorithm, γ is chosen to be a continuous function of z . The function has the form:

$$\gamma = \begin{cases} \gamma_0, & z \leq -\frac{\sigma}{2} \\ \gamma_0 + m(z + \frac{\sigma}{2}), & -\frac{\sigma}{2} \leq z \leq \frac{\sigma}{2} \\ \gamma_{0p}, & \frac{\sigma}{2} \leq z \leq L - \frac{\sigma}{2} \\ \gamma_0 + m(L + \frac{\sigma}{2} - z), & L - \frac{\sigma}{2} \leq z \leq L + \frac{\sigma}{2} \\ \gamma_0, & z \geq L + \frac{\sigma}{2} \end{cases} \quad (5)$$

where $m \equiv (\gamma_{0p} - \gamma_0)/\sigma$. The variation of γ with z is illustrated in Fig. 1.

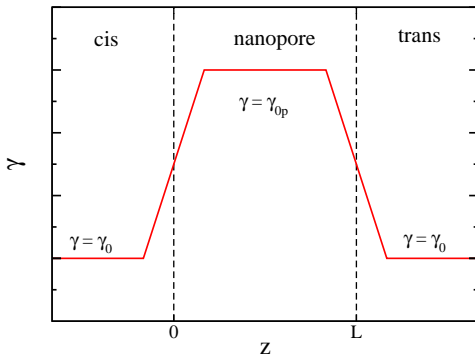


FIG. 1. Variation of the monomer friction coefficient, γ , with z . Note that γ varies continuously from γ_0 outside the pore to γ_{0p} inside the pore. The transition zones are centered at the pore edges and have a width of $\Delta z = \sigma$.

The degree to which the polymer has translocated across the nanopore is quantified using a translocation coordinate, s . This coordinate is defined in a manner similar to that of most other translocation studies, though with some slight differences. It is defined in relation to another coordinate, s' , which is chosen to be the number of bonds that have crossed the mid-point of the nanopore at $z = L/2$. Typically, one bond crosses this point, and this bond contributes to s' the fraction that lies on the *trans* side of the point. This is determined by the z coordinates of the monomers connected by this bond. Note that s' is a continuous variable in the range $s' \in [0, N-1]$. The coordinate s is given by $s = s' - n_p/2$, where n_p is the number of bonds spanning the nanopore when filled. It is defined $n_p \equiv L/\Delta z_p$, where Δz_p is average bond length projected along the nanopore z axis. In this study, the pore is sufficiently narrow that the polymer is strongly aligned inside, and simulations yield a value of $\Delta z_p = 0.96\sigma$, which is also the equilibrium bond length of the polymer. From this definition of s , the range $[0, N-1]$ corresponds to the translocation stage when the nanopore is filled. To complete the definition

of s for the case where the pore is less than half full (i.e. no bonds cross the mid-point of the pore), we define $s = -(n_p/2 - z_1/\Delta z_p)$, where z_1 is the coordinate of the end monomer. Likewise, in the case where less than half filled pore during emptying, $s = N-1 - (z_N - L)/\Delta z_p$, where z_N is the coordinate of the other end. With this definition of s , the following domains can be identified: (i) the pore filling stage for $s \in [-n_p, 0]$; (ii) the filled pore stage for $s \in [0, N-1-n_p]$; and the pore-emptying stage for $s \in [N-1-n_p, N-1]$. This is illustrated in Fig. 2.

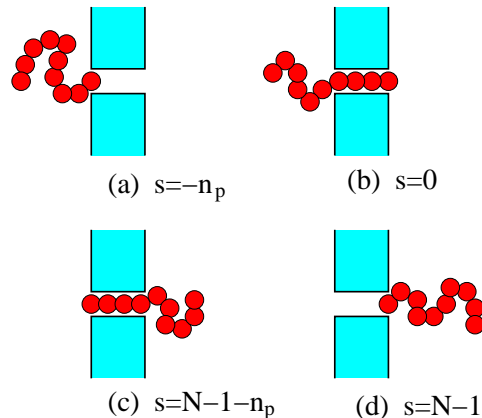


FIG. 2. Illustration showing translocation coordinate s at different points during translocation. The pore-filling stage lies between states (a) and (b), the transfer (i.e. filled pore) stage lies between states (b) and (c), and the pore emptying stage lies between states (c) and (d). n_p is the average number of bonds spanning the nanopore, and N is the number of monomers.

In our previous work,^{69,70} we employed a different translocation coordinate, Q , which was defined solely in terms of the coordinates of the monomers. Thus, unlike the coordinate s , its calculation is straightforward and does not require *a posteriori* knowledge of the quantity Δz_p . However, it has the disadvantage that it does not vary linearly with monomer displacement along the pore during the pore filling and emptying stages. By contrast, a given change in s corresponds to the same displacement for monomers inside the pore for *all* stages of translocation.

III. FOKKER-PLANCK EQUATION AND THE FRICTION COEFFICIENT

In the quasi-static limit, the time-dependent translocation probability distribution, $\mathcal{P}(s, t)$, is governed by the Fokker-Planck equation. The general form of the equation is¹

$$\frac{\partial \mathcal{P}(s, t)}{\partial t} = \frac{\partial}{\partial s} \left(\frac{D}{k_B T} \frac{\partial F}{\partial s} \mathcal{P}(s, t) \right) + \frac{\partial}{\partial s} D \frac{\partial \mathcal{P}(s, t)}{\partial s}, \quad (6)$$

where k_B is Boltzmann's constant, T is temperature, and $F(s)$ is the equilibrium translocation free energy func-

tion. In this study, $F(s)$ is calculated using the MC simulation method described in Ref. 70 and in Section IV A below. In addition, D is an effective diffusion coefficient that can be used to define the polymer friction parameter γ_{pol} using the Einstein relation:

$$D = \frac{k_{\text{B}}T}{\gamma_{\text{pol}}}. \quad (7)$$

Generally, D and γ_{pol} depend on the translocation position, s .

To establish a relationship between γ_{pol} and the simulation parameter γ defined in Eq. (5), we consider only the case of very strong pore friction. In this limit, the overall friction of the polymer is dominated by the friction of the monomers inside the pore. If N_{eff} monomers lie inside the pore, then the total friction of these monomers (and thus the polymer) is approximately

$$\gamma_{\text{pol}} = N_{\text{eff}}\gamma_{0\text{p}}, \quad (8)$$

where $\gamma_{0\text{p}}$ was defined earlier. The quantity N_{eff} can be estimated

$$N_{\text{eff}} \approx L/\Delta z_{\text{p}}, \quad (9)$$

where Δz_{p} is the average distance along z between bonded monomers inside the pore. For the nanopore dimensions used here ($L = 3\sigma$ and $R = 0.65\sigma$), $\Delta z_{\text{p}} = 0.96\sigma$ for monomers pairs located with $z \in [0, L]$, for which $N_{\text{eff}} = 3.125$. However, this turns out to be a slight underestimate of the true pore friction γ_z . A more accurate value can be determined by calculating the total friction of the pore monomers using the expression for the monomer friction in Eq. (5), and averaging over coordinates of the monomers for different configurations of the system. These configurations can be obtained from equilibrium MC simulations described below in Section IV A. For a pore of dimensions $L = 3\sigma$ and $R = 0.65\sigma$, we find $N_{\text{eff}} \approx 3.2$.

In practice, the value of N_{eff} is defined by Eq. (8), where γ_{pol} is the polymer friction coefficient that provides the best fit to the simulation data. In this sense, N_{eff} is the effective number of monomers that are subject to the friction in the nanopore. Significant deviations from the estimate in Eq. (9) can be interpreted as a breakdown in the underlying assumptions of conformational equilibrium and/or negligible friction of monomers outside the pore. Furthermore, in the strong pore friction regime where $\gamma_{0\text{p}}$ is sufficiently large, γ_{pol} and, thus, N_{eff} should be independent of $\gamma_{0\text{p}}$. We use this fact to locate the quasi-equilibrium regime.

Consider the case of a partially filled nanopore, again in the limit of strong pore friction, $\gamma_{0\text{p}} \gg \gamma_0$ and a strong polymer alignment in the pore. Here, γ_{pol} is expected to vary with s . For example, γ_{pol} should decrease with decreasing s as the pore empties monomers on the *cis* side. However, from the variation of γ with position in Eq. (5) and illustrated in Fig. 1 it can be shown that the filled-pore value of γ_{pol} extends approximately to $s =$

$-0.5\sigma/\Delta z_{\text{p}}$ on the *cis* side and decreases approximately linearly with decreasing s to a value of $\gamma_{\text{pol}} = (\gamma_{0\text{p}} + \gamma_0)/2$ at $s = -n_{\text{p}}$. The value on the *trans* side is related by symmetry. MC simulations used to calculate $\gamma_{\text{pol}}(s)$ using Eq. (5) and averaging over polymer configurations show very good agreement with this approximation. We use this approximation for FP calculations that consider the pore-emptying stages.

Under the assumption that the polymer maintains a state of conformational quasi-equilibrium during translocation and that the pore friction dominates, the relations derived above can be used to solve the FP equation. One important quantity of interest that emerges from such a calculation is the translocation first passage time. Consider a domain bounded by $s = a$ and $s = b$. The first passage time, τ , for a polymer located at $s_0 \in [a, b]$ at time $t = 0$ to reach either boundary has a probability distribution given by¹

$$g(\tau; s_0) = -\frac{d}{d\tau} \int_a^b ds p(s, \tau; s_0, 0), \quad (10)$$

where $p(s, t; s', t')$ is the conditional probability that the polymer reaches a value s at time t given that it had a value of s' at an earlier time t' . For a Markov process, $p(s, t; s', t')$ also satisfies Eq. (6). For most calculations in this study, we choose $a = 0$ and $b = N - 1 - n_{\text{p}}$, i.e. the points at which monomers first empty the *trans* and *cis* sides, as illustrated in Fig. 2(b) and (c). Thus, $[a, b]$ is the maximum range of s for a filled nanopore.

IV. METHODS

A. Free Energy Calculations

Monte Carlo simulations employing the Metropolis algorithm and the self-consistent multiple histogram (SCMH) method⁸⁰ were used to calculate the free energy functions for the polymer-nanopore model described in Section II. A detailed description of the methodology is given in our recent article on the translocation of hard-sphere chains.⁷⁰ The MC calculations in this work are similar to those of Ref. 70. However, the choice of definition of the translocation coordinate here requires that the calculations be performed in two stages. In the first stage, we evaluate the free energy function in the range $s \in [-n_{\text{p}}/2, N - 1 - n_{\text{p}}/2]$. The bounds of this range correspond to the cases where an end monomer located at the centre of the pore. Thus, it includes the filled-pore stage, as well as half the filling and emptying stages. In this range, $s' = s - n_{\text{p}}$ is the number of bonds that have crossed the midpoint of the pore, as described in Section II. In the second stage, we calculate the free energy in the filling and emptying stages using the definition of s in terms of the position of the end monomers. The different pieces of the free energy functions are fitted together by imposing continuity at $s = -n_{\text{p}}/2$ and $s = N - 1 - n_{\text{p}}/2$.

To implement the SCMH method, we employ a “window potential”

$$W_i(s) = \begin{cases} \infty, & s < s_i^{\min} \\ 0, & s_i^{\min} < s < s_i^{\max} \\ \infty, & s > s_i^{\max} \end{cases} \quad (11)$$

where s_i^{\min} and s_i^{\max} are the limits that define the range of s for the i -th window. These restrictions on s are part of the acceptance criteria for the MC trial moves, and any proposed move which produces a configuration with a s value outside this range is rejected. Within each window of s , a probability distribution $p_i(s)$ is calculated in the simulation. The window potential width, $\Delta s \equiv s_i^{\max} - s_i^{\min}$, is chosen to be sufficiently small that the variation in F does not exceed a few $k_B T$. Adjacent windows overlap, and the SCMH algorithm uses the $p_i(s)$ histograms to reconstruct the unbiased distribution, $P(s)$. For further details, see Ref. 70.

The windows are chosen to overlap with half of the adjacent window, such that $s_i^{\max} = s_{i+2}^{\min}$. In the first stage of the calculation, the window widths were typically $\Delta s/(N-1) = 0.02$, which required a total of $n_{\text{win}} = 99$ overlapping windows to span the range $s \in [-n_p/2, N-1-n_p/2]$. In addition, individual probability histograms were constructed using the binning technique. We used 20 bins per histogram and so the sampling bin width was $\delta s/(N-1) = 0.001$. For calculation of the free energy for values of s outside this range, the same parameters were used, except that a smaller number of windows was required.

The polymer configurations were generated by a random choice of three different particle moves. In one case, randomly chosen monomers were randomly displaced in each dimension. The displacement was chosen from a uniform distribution in the range $[-\Delta_{\text{max}}, \Delta_{\text{max}}]$. The trial moves were accepted with a probability $p_{\text{acc}} = \min(1, e^{-\Delta E/k_B T})$, where ΔE is the energy difference between the trial and current states. The maximum displacement parameter was chosen to be $\Delta_{\text{max}} = 0.07\sigma$, which yielded an acceptance probability of approximately 46%. In addition to single-monomer displacement, we also used crankshaft rotations, as well as uniform random translation of all monomers collectively. The maximum angular and translational displacements were chosen to yield comparably reasonable acceptance ratios. At the beginning of each simulation, the polymer was placed in a linear conformation at a position in the pore such that $s \in [s_i^{\min}, s_i^{\max}]$ for window i . The polymer was equilibrated for an appropriate period prior to the sampling for the calculation of the histograms. As an illustration, for a chain of length $N = 41$, the equilibration time was 2×10^7 MC cycles, and the production run time was 8×10^8 MC cycles. A MC cycle corresponds to an attempt to move each monomer an average of one time for each type of move.

B. Brownian Dynamics Simulations

We employ the BD simulation method to calculate translocation time distributions. For this method, the coordinates of the i th particle are advanced through a time Δt according to the algorithm:

$$x_i(t + \Delta t) = x_i(t) + \left(\frac{f_{i,x}}{\gamma_i} + k_B T \frac{d\gamma_i^{-1}}{dz} \right) \Delta t + \sqrt{2k_B T \Delta t / \gamma_i} \Delta w, \quad (12)$$

and likewise for y_i and z_i . Here, $f_{i,x}$ is the x -component of the conservative force on particle i . In addition, Δw is a random quantity drawn from a Gaussian of unit variance. The term proportional to the derivative $d\gamma_i^{-1}/dz$ accounts for the variation of the friction during the passage of a monomer through the pore. In practice, it is non-zero only near the *cis* and *trans* edges of the pore, as is evident in Fig. 1 and Eq. (5).

For each translocation event simulation, the polymer was initially placed in a linear conformation at a position corresponding to some desired initial coordinate, s_0 . The monomer closest to the centre of the nanopore was tethered to its initial position with a strong harmonic “pinning” force, and the coordinates of all the monomers evolved according to Eq. (12) until conformational equilibrium was reached. The time required for equilibration was dependent on the chain length, N , and on s_0 . Generally, longer *cis* or *trans* subchains required longer equilibration times. An appropriate time was determined by measuring the conformational correlation times measured for chains tethered to a flat surface in a series of separate simulations. As expected, the correlation times for the tethered chains scaled as $N^{1+2\nu} \approx N^{2.2}$, the same as that for a free Rouse chain. The equilibration time for the translocation simulations was chosen to be several times longer than the correlation time for a tethered chain of a length equal to that of the longer of the two subchains.

Following equilibration, the pinning force was turned off, and the dynamics of the polymer proceeded until the first time at which all monomers exited the pore on either the *cis* or *trans* side. We call the time taken for this complete emptying of the nanopore the translocation time, τ . In addition to this, we measure the first time, τ_1 , when all monomers have completely emptied either the *cis* or *trans* compartment. Clearly, $\tau_1 < \tau$. In this study, we focus mainly on the time τ_1 .

For any given set of system parameter values, many different translocation simulations were carried out. The number of translocation events was in the range of 10^3 – 10^5 . These simulations were used to calculate mean translocation time, $\langle \tau_1 \rangle$, and translocation time distributions, $g(\tau_1)$.

All simulations were carried out at a temperature $k_B T/\epsilon = 1$. The time step used in Eq. (12) was $\Delta t = 0.0001\gamma_0\sigma^2/\epsilon$. Most calculations used a nanopore of dimensions $L = 3\sigma$ and $R = 0.65\sigma$.

C. Theoretical Calculations

Using the free energy function calculated from the MC simulations, Eq. (6) was solved for a selected initial coordinate s_0 . This calculation was carried out using a standard finite-difference method with a “spatial” increment of $\Delta s/(N-1) = 0.001$ and a time increment of $\Delta t = 0.0001\gamma_0\sigma^2/\epsilon$. Adsorbing boundary conditions at $s = 0$ and $s = N-1-n_p$ were used in calculations for τ_1 . The calculation yielded a histogram approximation for $P(s, t)$, or, equivalently, the quantity $p(s, t; s_0, 0)$ in Eq. (10). The distribution of first passage times, $g(\tau_1; s_0)$, was calculated by solving Eq. (10). The integral was solved numerically using the trapezoid rule, and the derivative was calculated using a finite-difference approximation. The distribution function is dependent on the parameter N_{eff} . This quantity was adjusted to provide the best fit to the distribution measured directly from the BD simulations.

D. Units

For the model used in this study, the defining quantities of measure are σ , ϵ and γ_0 . Thus, length is measured in units of σ , energy in units of ϵ , friction in units of γ_0 , force in units of ϵ/σ , and time in units of $\gamma_0\sigma^2/\epsilon$. The results below are presented using this set of units.

V. RESULTS

Free energy functions were calculated using the MC method described in Section IV A. Sample free energy functions are shown in Fig. 3 for a polymer of length $N = 41$ in a nanopore of radius $R = 0.65$. The curves in Fig. 3(a) correspond to the case of unforced translocation. Data for pore lengths of $L = 3$ and $L = 3.5$ are shown. The curves are qualitatively similar to those calculated for translocation of hard-sphere chains in Ref. 70. The sharp increase and decrease of the function on either side correspond (mostly) to the pore-filling and pore-emptying stages of translocation, respectively. The wide and slightly curved plateau corresponds to the transfer stage, where the lengths of the *cis* and *trans* subchains decrease and increase, respectively, as monomers move through a filled pore. The symmetry of the functions reflects the underlying symmetry of the model in the absence of a driving force. The free energy barrier is higher for $L = 3.5$ than for $L = 3$ since a longer nanopore corresponds to greater confinement, and thus lower conformational entropy, in the filled-pore state. The ratio of the barrier heights is ≈ 0.86 , which is equal to the ratio of the nanopore lengths. This is in accord with the expectation that the free energy barrier height be proportional to the pore length.⁷⁰ In addition, the $L = 3.5$ curve has oscillations with a period of $\Delta s = 1$ and an amplitude of $\beta\Delta F_{\text{osc}} \approx 0.8$. This feature is also present in the $L = 3$

curve, but the amplitude is much smaller and the oscillations are barely detectable in the plot. These oscillations are an artifact of the model due to the variation of the orientational entropy of bonds passing through the *cis* and *trans* edges of the pore. This effect was discussed at length in Ref. 70. The variation of ΔF_{osc} with L follows a similar trend as in that study. In addition, the oscillation amplitude decreases with increasing R , in agreement with the results of Ref. 70 (data not shown). Figure 3(b) shows a free energy curve for driven translocation for a driving force of $f_d = 1$. This force causes the *trans* side to be energetically favoured to a considerable degree relative to the *cis* side.

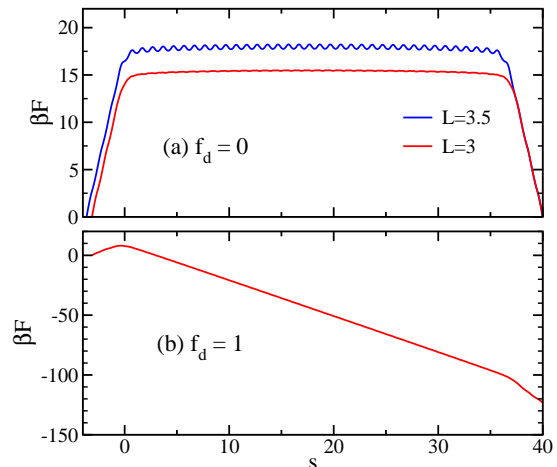


FIG. 3. Free energy functions for a polymer of length $N = 41$ and a pore of radius $R = 0.65$. Results are shown in (a) for non-driven translocation (i.e. $f_d = 0$) for pore lengths of $L = 3.5$ and $L = 3$. The results in (b) are for driven translocation for a driving force of $f_d = 1$ and a pore length of $L = 3$.

Let us consider further the free energy functions for unforced translocation. The derivation of the standard analytical approximation for the entropic barrier employs the result that the partition function for a self-avoiding polymer tethered to a hard wall has the form⁸¹

$$Z = (e^{-\beta\mu})^n n^{\lambda-1}, \quad (13)$$

where n is the length of the chain and μ is the chemical potential per monomer. In addition, the scaling exponent λ has a value of $\lambda \approx 0.69$ for a self-avoiding flexible polymer.⁸² For a polymer translocating through a short nanopore, the configurational partition function is a product of two terms, each of the form of Eq. (13), for the *cis* and *trans* subchains.¹ Following this approach, de Haan and Slater have noted that the free energy function for a pore of vanishing length is given by³⁴

$$\beta F(s/N) = (1-\lambda) \ln [(1-s/N)(s/N)], \quad (14)$$

where s is the number of monomers that have translocated through the pore. Thus, the free energy is a universal function of the scaled variable s/N . In the case

where the diffusion coefficient D in the FP equation is independent of s (i.e. pore friction is dominant), the FP formalism predicts³⁴ that such a free energy corresponds to a translocation first mean passage time that scales as $\langle \tau \rangle \sim N^2$.

For a finite-length nanopore, the situation is somewhat more complicated, since D (and thus γ_{pol}) changes during the pore-filling and emptying stages. Thus, D is constant only during the stage when the pore is filled, where $s \in [0, N']$, where $N' \equiv N - 1 - n_p$ is equal to the total number of bonds that lie outside the nanopore. In this domain, it is straightforward to show that the free energy satisfies a form similar to that of Eq. (14):

$$\beta F(s/N') = (1 - \lambda) \ln[(1 - s/N')(s/N')], \quad (15)$$

neglecting terms constant with respect to s . Thus, during the filled-pore stage, the free energy is predicted to be a universal function of s/N' . Note that this result can be shown to be consistent with the second term in Eq. (40) of Ref. 70. The polymer first reaches either bound in this range at the time τ_1 , as defined earlier. The quantity N' can be considered the effective length of the polymer for the filled-pore stage of translocation.

Figure 4 shows free energy functions for three different polymer lengths plotted as a function of s/N' for a nanopore of length $L = 3$ and radius $R = 0.65$. Note that functions are only shown for the filled-pore stage. In addition the curves have been shifted along the vertical axis so that the functions have approximately the same value at the mid-point of $s/N' = 0.5$. Also shown in the figure is the analytical prediction of Eq. (15). The simulation curves each display weak oscillations that were noted earlier. Note that the pore length L has been chosen to minimize the oscillation amplitude. The oscillations are more clearly visible in the enlargement in the inset of the figure. Since the period of the oscillations is $\Delta s = 1$, the oscillation period with respect to the scaled coordinate, s/N' , decreases as N increases. The model used to provide the analytical prediction does not incorporate the feature that gives rise to the oscillations, and so the theoretical curve is smooth, as expected. Apart from the oscillations, the calculated free energy functions overlap to a remarkable degree for the range of N considered. The theoretical curve is close to, but somewhat narrower than the simulation curves. This slight discrepancy is probably due to a finite size effect, since the derivations of Eqs. (14) and (15) use Eq. (13), a scaling relation is valid in the limit of very long polymers. It is expected that the calculated free energies will gradually approach the theoretical prediction with as N is increased to much larger values.

The calculated free energy functions can be used to solve the FP equation in order to calculate translocation time distributions. These calculations also use the expressions for the friction coefficient, γ_{pol} , derived in Section III. However, this approach is valid only when the pore friction dominates and when the polymer is in conformational equilibrium. One useful means to determine

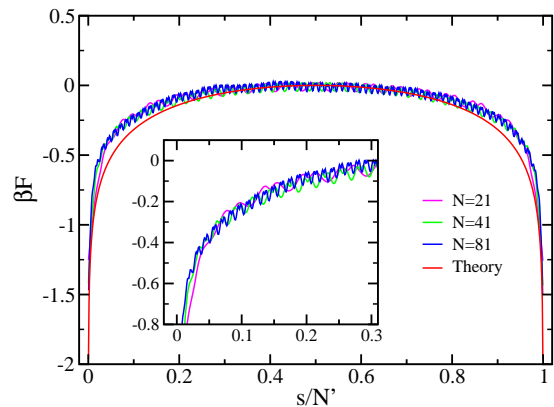


FIG. 4. Free energy vs s/N' . s is the number of monomers that have entered the pore just after the pore is filled, and $N' \equiv N - 1 - n_p$ is the number of bonds outside the nanopore, as described in the text. The graph shows results for three different polymer lengths calculated from MC SCM simulation. Also shown is the theoretical prediction of Eq. (15). The inset shows a close up near the edge of the profile.

where these conditions hold is to examine the scaling of the translocation time with chain length. Simulation studies of translocation generally yield power laws of the form $\langle \tau \rangle \sim N^\alpha$. Measurements of the exponent α have yielded a range of values, and the exponent appears to be sensitive to the pore geometry and finite-size effects. When the translocation time is sufficiently long relative to the relaxation time of the chain, the value predicted using the FP method is expected. For unforced translocation, the FP method gives $\alpha = 2$, while in the case of a strong driving force, $\alpha = 1$. Recently, simulations of unforced translocation observed $\alpha = 2$, in one case by decreasing the viscosity of the solvent (and thus shortening the polymer relaxation time),⁸³ and in the other case by increasing the pore friction.⁶⁹ In the present model, a sufficiently large pore friction, γ_{0p} , should slow translocation to the point where the FP result is observed.

As noted earlier, the FP prediction of $\alpha = 2$ for unforced translocation is expected for two conditions: (i) a constant D (i.e. constant γ_{pol}) in the FP equation, and (ii) the free energy is a universal function of either s/N (pores of zero length) or s/N' (finite-length pores). For a finite-length pore, D is constant in the filled-pore regime, within which F is approximately a universal function of s/N' for the range of N considered in Fig. 4 ($21 \leq N \leq 81$), though slightly different from the form predicted by Eq. (15). The oscillations in the curves for $L = 3$ in Fig. 4 are probably small enough to have a negligible effect on the translocation dynamics. Thus, the appropriate scaling test for quasi-static conditions for finite-length pores is

$$\langle \tau_1 \rangle \propto (N - N_p)^\alpha, \quad (16)$$

where the time τ_1 is the first time where the monomers have completely emptied from the *cis* or *trans* domains (as illustrated in Fig. 2(b) and (c)). Over this time in-

terval, the pore remains filled and D is constant. Also, N_p is the average number of monomers that lie inside a filled nanopore. For $R = 0.65$ and $L = 3$, $N_p = 4.125$. Thus, the quantity $N - N_p$ is the effective length of the polymer during this stage of translocation (i.e. number of monomers that pass through the nanopore during this stage of translocation). In the regime of sufficiently long chains and/or short pore length, the exponents obtained from this relation should be identical to those from $\langle \tau \rangle \propto N^\alpha$.

Figure 5 shows the scaling of $\langle \tau_1 \rangle$ with chain length for several different values of the pore friction parameter, γ_{0p} . As expected, decreasing γ_{0p} increases the translocation time. Over the range of chain lengths considered ($N = 21-61$), the power law of Eq. (16) is satisfied. In addition, as shown in the inset of the figure, α varies with γ_{0p} . At $\gamma_{0p} = \gamma_0 = 1$, $\alpha = 2.30$. As γ_{0p} increases and the pore friction becomes increasingly dominant, α monotonically decreases. At $\gamma_{0p} = 24$, the exponent is $\alpha = 1.99 \pm 0.02$, which is consistent with the FP prediction and indicates that the system is in the quasi-static regime. At higher γ_{0p} , the system will remain in this regime, and the exponent is expected to maintain a value close to $\alpha = 2$. This scaling behaviour is generally consistent with that of the MC dynamics simulations in Ref. 69, where the pore friction was tuned by varying the pore radius. In addition, these results closely parallel those of Ref. 66, where decreasing the solvent viscosity in that study has the same effect on α as increasing the pore friction in the present work. It is important to note that the measured exponents are valid only for the range of polymer lengths considered here. As the polymer length increases, the relaxation time of the polymer also increases, and a greater γ_{0p} will be required to maintain quasi-static conditions. For any pore friction corresponding to this regime for short polymers, increasing N will eventually push the system out of equilibrium, and the scaling exponent will change.

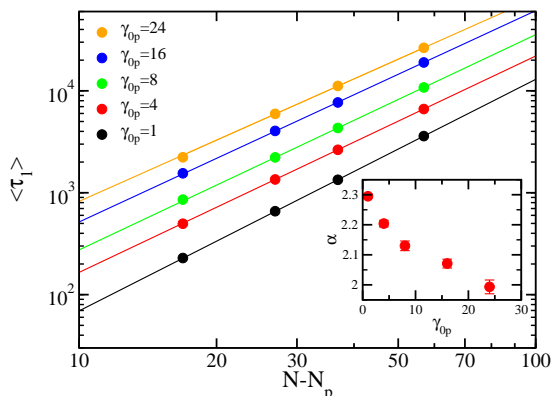


FIG. 5. Mean translocation time, $\langle \tau_1 \rangle$, vs $N - N_p$, for several different values of pore monomer friction coefficient, γ_{0p} . The polymer starts midway in the pore, with $s_0 = (N - 1 - n_p)/2$. In addition, $L = 3$, $R = 0.65$, and $f_d = 0$. The inset shows the translocation time scaling exponent, α , vs γ_{0p} .

Translocation time distributions calculated from BD simulations for a $N = 21$ polymer are shown in Fig. 6. The distributions stretch to higher translocation times as the pore friction increases, as expected. Overlaid on the BD curves are distributions predicted using the FP method. As explained in Section III, the friction coefficient, γ_{pol} , is parameterized by N_{eff} . This quantity is the effective number of monomers whose dynamics is governed by friction inside the pore. The theoretical curves have been calculated using values of N_{eff} that provide the best match between the theoretical and BD distributions. The theoretical curves are in excellent agreement with the simulation data. For lower values of the pore friction, the scaling results of Fig. 5 yield $\alpha > 2$, indicating that at least one of the two conditions for FP validity is not met. This fact is also evident in the variation of N_{eff} with pore friction shown in the inset of the figure. N_{eff} decreases with γ_{0p} but levels off to a value near $N_{eff} \approx 3.25$ at high γ_{0p} . This value is close to the approximation in Eq. (9) and even closer to the value of $N_{eff} = 3.2$ measured directly from MC simulations, as described in Section III. As noted earlier, any appreciable deviation from this prediction indicates a breakdown of the condition of conformational quasi-equilibrium and/or the dominance of pore friction. As the pore friction increases in strength, these two conditions become increasingly valid, as evident from the N_{eff} values. These results and conclusions are consistent with those observed in our recent MC dynamics translocation study.⁷⁰

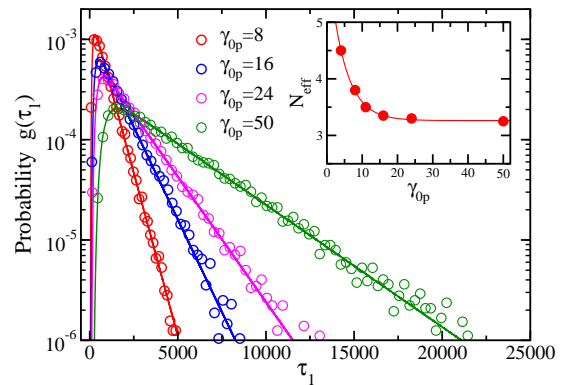


FIG. 6. Translocation time distributions for unforced translocation where the polymer starts midway in the nanopore, with $s_0 = (N - 1 - n_p)/2$. In addition, $L = 3$, $R = 0.65$, and $f_d = 0$. The open circles denote BD simulation data, and the solid curves show FP theoretical predictions. The inset shows N_{eff} vs γ_{0p} , for N_{eff} values that provide the best match between the FP predictions and BD data. The solid line is a guide for the eye.

It is a curious fact that it is possible for the FP distributions to be in such excellent agreement with the BD distributions even outside the regime where the conditions required for the theory to be valid hold (e.g. at $\gamma_{0p} = 8$). Thus, the functional form of the measured distributions provide no clear indication of where the correct

regime lies. This demonstrates the importance of employing complementary measurements of other relevant quantities, such as α . It also demonstrates the importance of establishing a clear relation between the friction coefficient used in the FP equation and the related parameter(s) employed in the simulation model.

Now consider the pore emptying stage for unforced translocation. At time $t = \tau_1$, the polymer has just reached the point where the *cis* or *trans* domain has emptied, while at time $t = \tau$, the nanopore itself has just emptied. Thus, the pore emptying time can be defined as difference $\tau - \tau_1$. Figure 7 shows this time distribution for an $N = 21$ polymer moving through a pore with friction $\gamma_{0p} = 50$. From the result in Fig. 6, it is clear that this corresponds to a case where the polymer maintains conformational quasi-equilibrium during the filled-pore stage. However, it is not clear that this condition will be maintained during pore emptying. As is evident in the inset of the figure, which shows the free energy profile for the system, the free energy gradient is much larger here than during the filled stage. Consequently, the translocation rate is expected to be much greater, and this could result in conformational distortion of the *cis* and *trans* subchains. To test this condition, FP calculations were carried out using $s = 0$ as the initial state. The polymer friction $\gamma_{pol}(s)$ for the emptying stage was calculated using the method described in Section III. The calculations used the same value of $N_{\text{eff}} = 3.25$ used in the fit to the $\gamma_{0p} = 50$ curve in Fig. 6. The calculated distribution is shown as the solid curve in the figure, and is in excellent agreement with the results of the simulation. Evidently, the friction is large enough in this case to maintain quasi-static conditions.

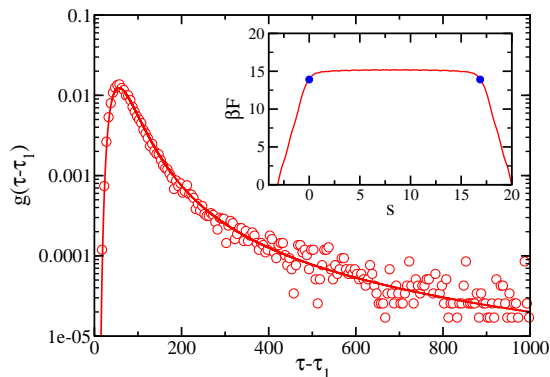


FIG. 7. Distribution of the pore emptying time $\tau - \tau_1$ for unforced translocation. In this stage, the polymer starts at $s = 0$ at time τ_1 and proceeds until the time τ , at which the nanopore is fully empty. The monomer pore friction is $\gamma_{0p} = 50$. In addition, $N = 21$, $L = 3$ and $R = 0.65$. The open circles denote BD simulation data, and the solid curve shows the FP theoretical prediction. The inset shows the free energy curve used in the calculation. The blue circles indicate the two possible starting points of the pore emptying stage.

Next, we consider the case of forced translocation. Fig-

ure 8 shows translocation time distributions for a $N = 41$ polymer subject to a driving force of $f_d = 1$. Results for several different values of γ_{0p} are shown. In these simulations, the polymer was initially placed at $s_0 = 2.04$. As evident in Fig. 3(b), this position is on the *trans* side of the free energy maximum located near $s = -0.33$. The translocation was sufficiently advanced to prevent the polymer exiting on the *cis* side. Most of the monomers initially lie in the *cis* compartment and are pushed through the nanopore during translocation.

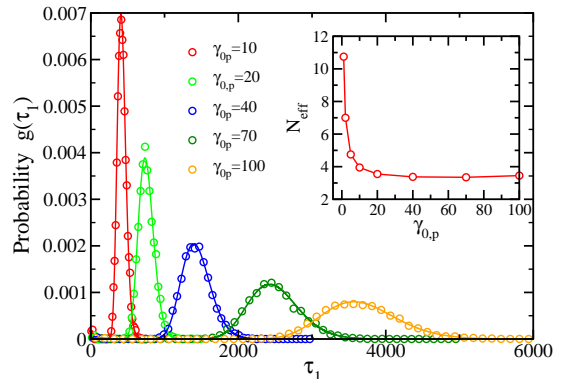


FIG. 8. Translocation time distributions for driven translocation for several values of γ_{0p} . The symbols denote BD simulation data and the solid curves show theoretical predictions using the FP formalism. The data are for a polymer of length $N = 41$ starting at $s_0 = 2.04$ and subject to a driving force of $f_d = 1$. In addition, the pore dimensions are $L = 3$ and $R = 0.65$. The inset shows N_{eff} vs γ_{0p} . These values of N_{eff} provided the best match between the FP and BD distributions.

The distributions are Gaussian-like, and they shift to longer times as the pore friction increases, as expected. In addition, the distribution width also increases with the pore friction strength. Overlaid on the BD distributions are theoretical curves calculated using the FP approach. The N_{eff} values used in the FP calculations are shown in the inset of the figure. As in the case of unforced translocation, the theoretical curves are in excellent agreement with the BD distributions for the data shown. In this case, quantitative agreement was not especially good at low pore friction, $\gamma_{0p} < 10$ (data not shown). These results are easily understood from examining the data in the inset. Consistent with the results shown in the inset of Fig. 6, N_{eff} is very high at low γ_{0p} , but decreases rapidly and levels off at a value of $N_{\text{eff}} = 3.35$ at high γ_{0p} . This limiting value is close to the expected value of $N_{\text{eff}} = 3.2$. The slight higher value measured from the simulation data is probably due to a residual contribution to the total polymer friction from the monomers outside the pore. To summarize, the FP distributions are in excellent agreement with the simulation data in the high pore-friction regime, where the theory is expected to work, and in poorer agreement with simulation outside this regime.

It is instructive to examine the conformational be-

haviour of the polymer during translocation directly. One useful measure is the displacement of the end monomer on the *cis* and *trans* sides from the centre of the nearest opening of the nanopore. The z components of these displacements are $Z_c = z_1$ and $Z_t = z_N - L$ respectively, where z_1 is the z coordinate of monomer 1, defined to be the last to go through the nanopore, and z_N is the coordinate of monomer N , defined to be the first to go through the pore.

Figure 9 shows variation of $\langle Z_c^2 \rangle$ and $\langle Z_t^2 \rangle$ with s during translocation. These results were obtained from the simulations used in Fig. 8. Results for several different γ_{0p} are shown. At low γ_{0p} , where translocation is rapid, there is a compression of the *trans* subchain. On this *cis* side, there is a corresponding lag in the response of the position of the polymer end to the pull of the polymer during translocation. These results are a direct measure of the out-of-equilibrium character of the polymer. The delayed response on the *cis* side is in keeping with the finite time required for the “tension front” to reach the *cis* end in the context of the tension propagation theory of translocation.^{45,67,71,72,74,75} As the pore friction increases, $\langle Z_t^2 \rangle$ monotonically increases and $\langle Z_c^2 \rangle$ decreases. Thus, the polymer tends toward conformational equilibrium. At $\gamma_{0p} \approx 70$, the polymer has reached conformational quasi-equilibrium. This is evident from the observed symmetry between the *cis* and *trans* curves at high γ_{0p} . Results of comparable calculations using the x and y components of the end-monomer displacements, as well as the radius of gyration of the *cis* and *trans* subchains, showed identical trends (data not shown). Finally, it should be noted that increases in both the polymer length and the driving force are expected push the system out of equilibrium. Thus, the degree of pore friction required to achieve quasi-equilibrium will increase as N increases and as f_d increases.

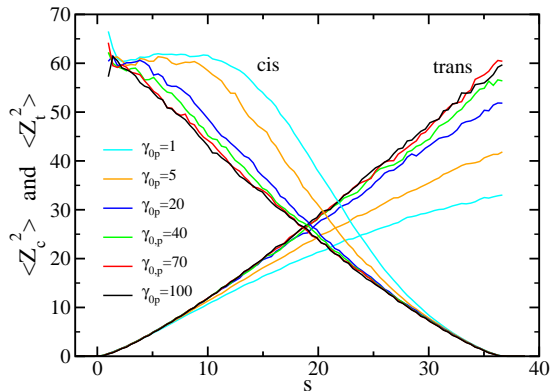


FIG. 9. $\langle Z_c^2 \rangle$ and $\langle Z_t^2 \rangle$ of the *cis* and *trans* subchains as a function of s several different values of γ_{0p} . The data are averages over many translocation events for a polymer of length $N = 41$ starting at $s_0 = 2.04$ and subject to a pore monomer driving force of $f_d = 1$. In addition, $L = 3$ and $R = 0.65$.

A close comparison of the results of Figs. 8 and 9 reveals an interesting point. Both sets of data show that

conformational quasi-equilibrium is approached as the pore friction strength increases. However, the variation of N_{eff} with γ_{0p} shows that the FP formalism appears to be valid at $\gamma_{0p} = 40$ and higher, while the direct measurement of the conformational state of the polymer shows the polymer is still somewhat out of equilibrium at $\gamma_{0p} = 40$. This shows that agreement between the FP predictions and simulation data (and, by extension, experimental data) does not provide a perfectly accurate test for the quasi-equilibrium condition as the system crosses over into this regime.

Figure 10 shows translocation time distributions for a $N = 41$ polymer for various driving forces. The pore friction strength is $\gamma_{0p} = 70$. The variation of $\langle Z_c^2 \rangle$ and $\langle Z_t^2 \rangle$ with s is the same for all values of f_d considered here (data not shown), indicating that the polymer is in conformational equilibrium over this range. Theoretical distributions were calculated for $N_{\text{eff}} = 3.35$ and are all in excellent agreement with the simulation data. The inset shows the variation of $\langle \tau_1 \rangle$ and $\langle \tau \rangle$ with f_d^{-1} . Fits to a power law $\langle \tau_1 \rangle \propto f_d^\delta$ yielded an exponent of $\delta = -0.984 \pm 0.006$. A fit of $\langle \tau \rangle$ to the same relation yielded the same scaling exponent. These results are very close to the prediction that $\langle \tau \rangle \propto f_d^{-1}$ by Muthukumar in the limit where pore friction dominates.²⁶ Note once again that increases in the both the driving force and the polymer length are expected to push the system out of equilibrium, leading to dynamical behaviour that diverges from that of the FP predictions. This is illustrated by recent MD simulations for a $N = 128$ polymer, which yield values of $\delta \approx -0.9$ for low and intermediate forces, and somewhat higher values (that depend on the details of the model) for strong forces.⁷⁵

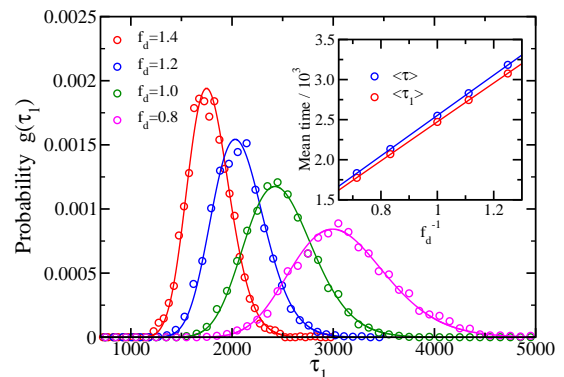


FIG. 10. Translocation time distributions for driven translocation for several values of the driving force, f_d . The symbols denote BD simulation data and the solid curves show theoretical predictions. The data are for a polymer of length $N = 41$ starting at $s_0 = 2.04$ and a pore with a friction of $\gamma_{0p} = 70$ and dimensions of $L = 3$ and $R = 0.65$. The FP curves were calculated using $N_{\text{eff}} = 3.35$. The inset shows $\langle \tau_1 \rangle$ and $\langle \tau \rangle$ vs f_d^{-1} . The solid lines are fits to the data using a power law functional form. The fits yielded a scaling of $f_d^{-0.984 \pm 0.006}$ for both $\langle \tau_1 \rangle$ and $\langle \tau \rangle$.

Finally, we examine the scaling of the translocation

time with polymer length, N . In the limit of very strong driving force and zero pore length, the FP approach predicts^{1,26} a scaling of $\langle\tau\rangle \propto N$. This corresponds to the case where the free energy function is dominated by the chemical potential difference across the pore and where the entropic barrier contribution is negligible. In this limit, the mean velocity is constant and thus the mean coordinate varies as $\langle s \rangle \propto t$, where t is the time measured from the beginning of the translocation process. Equivalently, it is expected that $\langle s - s_0 \rangle \propto t$ for an arbitrary initial coordinate s_0 . For translocation of chains of arbitrary length each located at the same s_0 at $t = 0$, it is then predicted that $\langle\tau_1\rangle \propto \Delta s$, where $\Delta s = N - 1 - n_p - s_0$ is the displacement during the time interval $[0, \tau_1]$.

To test this prediction, we measured translocation times τ_1 for chains of various lengths for $\gamma_{0p} = 70$, $f_d = 1$, and an initial coordinate value of $\Delta s = 3.44$. For these conditions and the range of lengths considered ($N = 21$ – 41) we know from the results shown in the figures above that the polymer will remain in conformational quasi-equilibrium. The inset of Fig. 11 shows that $\langle\tau_1\rangle$ does appear to vary linearly with Δs . A power law fit yields a scaling of $\langle\tau_1\rangle \propto \Delta s^{1.025 \pm 0.004}$. The slight deviation of the scaling exponent from unity may be a residual effect of the entropic contribution to the free energy barrier. Figure 11 also shows translocation time distributions for the different chain lengths. Overlaid are the theoretical predictions using the FP approach and the same value of $N_{\text{eff}} = 3.35$ used for calculations with results shown in Fig. 10. The predictions are in excellent agreement with the simulation results.

The FP scaling exponent for driven translocation of $\alpha = 1$ is only valid in a regime that is determined by values of the pore friction, polymer length and driving force. Outside the quasi-equilibrium regime, α is expected to deviate from this value. As noted earlier, BDTP calculations have shown that α varies with each these parameters, approaching a value of $\nu = 1 + \nu \approx 1.6$ in the limit of large N .⁷⁵ In the limit of high pore friction and low N , α tends toward a value of unity, suggesting that the FP regime considered in this study may be a limiting case of that theoretical model.

VI. CONCLUSIONS

In this study, we have used BD simulations to study the translocation dynamics of a coarse-grained polymer. These simulations differ from those of most other studies by the presence of a tunable friction parameter, γ_{0p} , for monomers that lie inside the pore. We have considered the case where $\gamma_{0p} \geq \gamma_0$, where γ_0 is the friction outside the pore, whereas other studies have essentially used $\gamma_{0p} = \gamma_0$. Increasing γ_{0p} reduces the rate of translocation. For low γ_{0p} , where translocation is rapid, the polymer conformation exhibits out-of-equilibrium conformational behaviour, while for sufficiently high γ_{0p} and slow translocation, a state of quasi-equilibrium is observed.

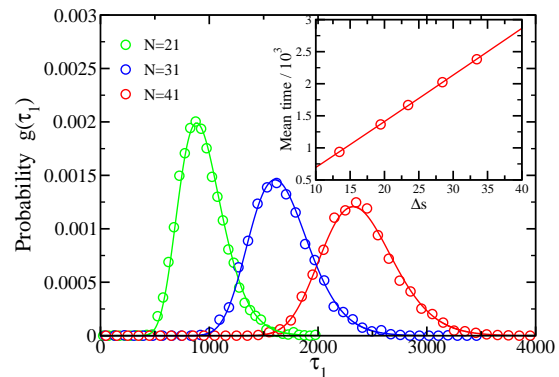


FIG. 11. Translocation time distributions $g(\tau_1)$ for driven translocation for polymers of several lengths. In each case translocation starts at $s_0 = 3.44$. In addition, $\gamma_{0p} = 70$ and $f_d = 1$. The symbols denote BD simulation data and the solid curves show theoretical predictions. The FP curves were calculated using $N_{\text{eff}} = 3.35$. The inset shows $\langle\tau_1\rangle$ vs Δs , where $\Delta s = N - 1 - n_p - s_0$. The solid line is a fit to the data using a power law. The fit yielded a scaling of $\langle\tau_1\rangle \propto \Delta s^{1.025 \pm 0.004}$.

We have examined the behaviour of the translocation time τ_1 on the pore friction, and have analyzed the data using the FP formalism together with translocation free energy functions that have been calculated explicitly using MC simulations.

Generally, the analysis of the data yield results that are consistent with the predictions of the FP approach for sufficiently strong pore friction, and poorer results for weaker pore friction. In the case of unforced translocation, the scaling exponent for $\langle\tau_1\rangle$ was measured to be $\alpha = 1.99 \pm 0.02$ for strong friction. This result has also been observed in Refs. 83 and 69 and is expected in the case where pore friction dominates and conformational quasi-equilibrium holds. In addition, for translocation driven by a strong force of strength f_d , we observed scalings very close to $\langle\tau_1\rangle \propto f_d^{-1}$ at sufficiently high γ_{0p} . Upon variation in the chain length N , we observed a scaling of approximately $\langle\tau_1\rangle \propto \Delta s$, where Δs is the translocation coordinate range between the initial value and the value when the *cis* region has just emptied. This provides indirect evidence for the validity of the scaling predicted by the FP approach of $\langle\tau\rangle \propto N$ in the limit of strong force and strong pore friction. As another test, FP calculations were used to analyze the translocation time distributions obtained from the BD simulations. These calculations use a total pore friction value that is parameterized by a quantity N_{eff} , the effective number monomers whose dynamics are strongly affected by the pore. For sufficiently strong pore friction, the FP distributions were in excellent agreement with those obtained from the simulations using physically meaningful values of N_{eff} .

The results of this study provide direct evidence that the FP formalism provides a valid description of polymer translocation dynamics in the regime where the translocation time is sufficiently long relative to the conforma-

tional relaxation time of the polymer. The pore friction strength required to maintain quasi-equilibrium is expected to increase with increasing polymer length and driving force. It will also be affected by incorporation of hydrodynamic correlations, which will change the relaxation time of the polymer. Delineation of the regime of validity for the FP equation in describing translocation dynamics would be illuminating but time consuming and is beyond the scope of the present study.

ACKNOWLEDGMENTS

JMP would like to thank Sheldon B. Opps for helpful discussions. This work was supported by the Natural Sciences and Engineering Research Council of Canada (NSERC). We are grateful to the Atlantic Computational Excellence Network (ACEnet) for use of their computational facilities.

- ¹M. Muthukumar, *Polymer Translocation* (CRC Press, Boca Raton, 2011).
- ²D. Panja, G. T. Barkema, and A. B. Kolomeisky, *J. Phys.: Condens. Matter* **25**, 413101 (2013).
- ³A. Milchev, *J. Phys.: Condens. Matter* **23**, 103101 (2011).
- ⁴B. Alberts, A. Johnson, J. Lewis, M. Raff, K. Roberts, and P. Walters, *Molecular Biology of the Cell*, 5th ed. (Garland Science, New York, 2008).
- ⁵H. Lodish, A. Berk, C. A. Kaiser, M. Krieger, A. Bretscher, H. Ploegh, A. Amon, and M. P. Scott, *Molecular Cell Biology*, seventh ed. (W. H. Freeman and Company, New York, 2012).
- ⁶J. J. Kasianowicz, E. Brandin, D. Branton, and D. W. Deamer, *Proc. Natl. Acad. Sci. U.S.A.* **93**, 13770 (1996).
- ⁷M. Akeson, D. Branton, J. Kasianowicz, E. Brandin, and D. Deamer, *Biophys. J.* **77**, 3227 (1999).
- ⁸A. Meller, L. Nivon, E. Brandin, J. Golovchenko, and D. Branton, *Proc. Natl. Acad. Sci. U.S.A.* **97**, 1079 (2000).
- ⁹A. Meller, *J. Phys.: Condens. Matter* **15**, R581 (2003).
- ¹⁰H. Wang, J. Dunning, A. Huang, J. Nyamwanda, and D. Branton, *Proc. Natl. Acad. Sci. U.S.A.* **101**, 13472 (2004).
- ¹¹T. Z. Butler, J. H. Gundlach, and M. A. Troll, *Biophys. J.* **90**, 190 (2006).
- ¹²C. T. A. Wong and M. Muthukumar, *J. Chem. Phys.* **128**, 154903 (2008).
- ¹³C. T. A. Wong and M. Muthukumar, *J. Chem. Phys.* **133**, 045101 (2010).
- ¹⁴J. Li, M. Gershow, D. Stein, E. Brandin, and J. Golovchenko, *Nature Mater.* **2**, 611 (2003).
- ¹⁵P. Chen, J. Gu, E. Brandin, Y. R. Kim, Q. Wang, and D. Branton, *Nano Lett.* **4**, 2293 (2004).
- ¹⁶D. Fologea, J. Uplinger, B. Thomas, D. McNabb, and J. Li, *Nano Lett.* **5**, 1734 (2005).
- ¹⁷D. Fologea, M. Gershow, B. Ledden, D. McNabb, J. Golovchenko, and J. Li, *Nano Lett.* **5**, 1905 (2005).
- ¹⁸A. J. Storm, C. Storm, J. Chen, H. Zandbergen, J.-F. Joanny, and C. Dekker, *Nano Lett.* **5**, 1193 (2005).
- ¹⁹A. Storm, J. Chen, H. Zandbergen, and C. Dekker, *Physical Review E* **71**, 051903 (2005).
- ²⁰R. Purnell, K. Mehta, and J. Schmidt, *Nano Letters* **8**, 3029 (2008).
- ²¹D. Branton, D. Deamer, A. Mirziali, H. Bayley, S. A. Benner, T. Butler, M. D. Ventra, S. Garaj, A. Hibbs, X. Huang, S. B. Jovanovich, P. S. Krstic, S. Lindsay, X. S. Ling, C. H. Mastrangelo, A. Meller, J. S. Oliver, Y. V. Pershin, J. M. Ramsey, R. Riehn, G. V. Soni, V. Tabard-Cossa, M. Wanunu, M. Wiggin, and J. A. Schloss, *Nat. Biotechnol.* **26**, 1146 (2008).
- ²²B. M. Venkatesan and R. Bashir, *Nat. Nanotech.* **6**, 615 (2011).
- ²³M. Wanunu, *Phys. Life Rev.* **9**, 125 (2012).
- ²⁴Y. Yang, R. Liu, H. Xie, Y. Hui, R. Jiao, Y. Gong, and Y. Zhang, *J. Nanosci. Nanotechnol.* **13**, 4521 (2013).
- ²⁵W. Sung and P. J. Park, *Phys. Rev. Lett.* **77**, 783 (1996).
- ²⁶M. Muthukumar, *J. Chem. Phys.* **111**, 10371 (1999).
- ²⁷E. Slonkina and A. B. Kolomeisky, *J. Chem. Phys.* **118**, 7112 (2003).
- ²⁸M. Muthukumar, *J. Chem. Phys.* **118**, 5174 (2003).
- ²⁹C. Y. Kong and M. Muthukumar, *J. Chem. Phys.* **120**, 3460 (2004).
- ³⁰D. Keijian, Z. Furu, C. Dongqin, and Y. Zengliang, *Biochem. Biophys. Res. Commun.* **341**, 139 (2006).
- ³¹M. G. Gauthier and G. W. Slater, *J. Chem. Phys.* **128**, 065103 (2008).
- ³²M. G. Gauthier and G. W. Slater, *J. Chem. Phys.* **128**, 205103 (2008).
- ³³A. Mohan, A. B. Kolomeisky, and M. Pasquali, *J. Chem. Phys.* **133**, 024902 (2010).
- ³⁴H. W. de Haan and G. W. Slater, *J. Chem. Phys.* **134**, 154905 (2011).
- ³⁵S. Yang and A. V. Neimark, *J. Chem. Phys.* **136**, 214901 (2012).
- ³⁶S. Zhang, C. Wang, L.-Z. Sun, C.-Y. Li, and M.-B. Luo, *J. Chem. Phys.* **139**, 044902 (2013).
- ³⁷M. Wanunu, J. S. Sutina, B. McNally, A. Chow, and A. Meller, *Biophys. J.* **95**, 4716 (2008).
- ³⁸J. Chuang, Y. Kantor, and M. Kardar, *Phys. Rev. E* **65**, 011802 (2001).
- ³⁹Y. Kantor and M. Kardar, *Phys. Rev. E* **69**, 021806 (2004).
- ⁴⁰K. Luo, I. Huopaniemi, T. Ala-Nissila, and S.-C. Ying, *J. Chem. Phys.* **124**, 114704 (2006).
- ⁴¹M. G. Gauthier and G. W. Slater, *Phys. Rev. E* **79**, 021802 (2009).
- ⁴²A. Bhattacharya, W. H. Morrison, K. Luo, T. Ala-Nissila, S.-C. Ying, A. Milchev, and K. Binder, *Eur. Phys. J. E* **29**, 423 (2009).
- ⁴³K. Luo and R. Metzler, *Phys. Rev. E* **82**, 021922 (2010).
- ⁴⁴A. Bhattacharya and K. Binder, *Phys. Rev. E* **81**, 041804 (2010).
- ⁴⁵J. L. A. Dubbeldam, V. G. Rostiashvili, A. Milchev, and T. A. Vilgis, *Phys. Rev. E* **85**, 041801 (2012).
- ⁴⁶J. Feng, Y. Shang, L. Zhou, H. Liu, and Y. Hu, *Chin. J. Chem. Eng.* **20**, 231 (2012).
- ⁴⁷A. Milchev, K. Binder, and A. Bhattacharya, *J. Chem. Phys.* **121**, 6042 (2004).
- ⁴⁸S. Tsuchiya and A. Matsuyama, *Phys. Rev. E* **76**, 011801 (2007).
- ⁴⁹K. Luo, T. Ala-Nissila, and S.-C. Ying, *J. Chem. Phys.* **124**, 034714 (2006).
- ⁵⁰J. K. Wolterink, G. T. Barkema, and D. Panja, *Phys. Rev. Lett.* **96**, 208301 (2006).
- ⁵¹S. Guillouze and G. W. Slater, *Phys. Lett. A* **359**, 261 (2006).
- ⁵²J. L. A. Dubbeldam, A. Milchev, V. G. Rostiashvili, and T. A. Vilgis, *Phys. Rev. E* **76**, 010801(R) (2007).
- ⁵³J. L. A. Dubbeldam, A. Milchev, V. G. Rostiashvili, and T. A. Vilgis, *EPL* **79**, 18002 (2007).
- ⁵⁴I. Huopaniemi, K. Luo, T. Ala-Nissila, and S.-C. Ying, *Phys. Rev. E* **75**, 061912 (2007).
- ⁵⁵D. Panja, G. T. Barkema, and R. C. Ball, *J. Phys.: Condens. Matter* **19**, 432202 (2007).
- ⁵⁶D. Panja, G. T. Barkema, and R. C. Ball, *J. Phys.: Condens. Matter* **20**, 075101 (2008).
- ⁵⁷D. Wei, W. Yang, X. Jin, and Q. Liao, *J. Chem. Phys.* **126**, 204901 (2007).
- ⁵⁸K. Luo, S. T. T. Ollila, I. Huopaniemi, T. Ala-Nissila, P. Pormski, M. Karttunen, S.-C. Ying, and A. Bhattacharya, *Phys. Rev. E* **78**, 050901(R) (2008).
- ⁵⁹H. Vocks, D. Panja, G. T. Barkema, and R. C. Ball, *J. Phys.: Condens. Matter* **20**, 095224 (2008).
- ⁶⁰V. V. Lehtola, R. P. Linna, and K. Kaski, *Phys. Rev. E* **78**, 061803 (2008).
- ⁶¹V. V. Lehtola, R. P. Linna, and K. Kaski, *EPL* **85**, 58006 (2009).
- ⁶²K. Luo, T. Ala-Nissila, S.-C. Ying, and R. Metzler, *EPL* **88**, 68006 (2009).

- ⁶³F. Kapahnke, U. Schmidt, D. W. Heermann, and M. Weiss, J. Chem. Phys. **132**, 164904 (2010).
- ⁶⁴H. W. de Haan and G. W. Slater, Phys. Rev. E **81**, 051802 (2010).
- ⁶⁵J. L. A. Dubbeldam, V. G. Rostiashvili, A. Milchev, and T. A. Vilgis, Phys. Rev. E **83**, 011802 (2011).
- ⁶⁶H. W. de Haan and G. W. Slater, J. Chem. Phys. **136**, 154903 (2012).
- ⁶⁷T. Ikonen, A. Bhattacharya, T. Ala-Nissila, and W. Sung, Phys. Rev. E **85**, 051803 (2012).
- ⁶⁸C. M. Edmonds, P. J. Hesketh, and S. Nair, Chem. Phys. **425**, 1 (2013).
- ⁶⁹J. M. Polson and A. C. M. McCaffrey, J. Chem. Phys. **138**, 174902 (2013).
- ⁷⁰J. M. Polson, M. Fatehi Hassanabad, and A. C. M. McCaffrey, J. Chem. Phys. **138**, 024906 (2013).
- ⁷¹T. Sakaue, Phys. Rev. E **76**, 021803 (2007).
- ⁷²T. Sakaue, Phys. Rev. E **81**, 041808 (2010).
- ⁷³T. Saito and T. Sakaue, Eur. Phys. J. E **34**, 135 (2011).
- ⁷⁴P. Rowghanian and A. Y. Grosberg, J. Phys. Chem. B **115**, 14127 (2011).
- ⁷⁵T. Ikonen, A. Bhattacharya, T. Ala-Nissila, and W. Sung, J. Chem. Phys. **137**, 085101 (2012).
- ⁷⁶T. Ikonen, A. Bhattacharya, T. Ala-Nissila, and W. Sung, arXiv preprint arXiv:1211.7043 (2012).
- ⁷⁷T. Saito and T. Sakaue, Eur. Phys. J. E **35**, 125 (2012).
- ⁷⁸T. Ikonen, A. Bhattacharya, T. Ala-Nissila, and W. Sung, EPL **103**, 38001 (2013).
- ⁷⁹R. B. Bird, C. F. Curtiss, R. C. Armstrong, and H. O., *Dynamics of Polymeric Liquids, Volume 2, Kinetic Theory*, 2nd ed. (Wiley, New York, 1987).
- ⁸⁰D. Frenkel and B. Smit, *Understanding Molecular Simulation: From Algorithms to Applications*, 2nd ed. (Academic Press, London, 2002) Chap. 7.
- ⁸¹P.-G. de Gennes, *Scaling Concept in Polymer Physics* (Cornell University Press, London, 1979).
- ⁸²E. Eisenriegler, K. Kremer, and K. Binder, J. Chem. Phys. **77**, 6296 (1982).
- ⁸³H. W. de Haan and G. W. Slater, J. Chem. Phys. **136**, 204902 (2012).